HHS Public Access

Author manuscript

Lab Chip. Author manuscript; available in PMC 2019 May 15.

Published in final edited form as:

Lab Chip. 2018 May 15; 18(10): 1485–1493. doi:10.1039/c8lc00168e.

"Dip-and-read" paper-based analytical devices using distance-based detection with color screening

Kentaro Yamada[a,b], **Daniel Citterio**[b], and **Charles S. Henry**[a]

[a]Department of Chemistry, Colorado State University, Fort Collins, Colorado 80523, USA

[b]Department of Applied Chemistry, Keio University, 3-14-1 Hiyoshi, Kohoku-ku, Yokohama 223-8522, Japan

Abstract

An improved paper-based analytical device (PAD) using color screening to enhance device performance is described. Current detection methods for PADs relying on the distance-based signalling motif can be slow due to the assay time being limited by capillary flow rates that wick fluid through the detection zone. For traditional distance-based detection motifs, analysis can take up to 45 min for a channel length of 5 cm. By using a color screening method, quantitation using distance-based PAD can be achieved in minutes using a "dip-and-read" approach. A colorimetric indicator line deposited onto a paper substrate using inkjet-printing undergoes a concentration-dependent colorimetric response for a given analyte. This color intensity-based response has been converted to a distance-based signal by overlaying a color filter with a continuous color intensity gradient matching the color of the developed indicator line. As a proof-of-concept, Ni quantification in welding fume was performed as a model assay. The results of multiple independent user testing gave the mean absolute percentage error and average relative standard deviations of 10.5% and 11.2% respectively, which were an improvement upon analysis based on simple visual color comparison with a read guide (12.2%, 14.9%). In addition to the analytical performance comparison, an interference study and a shelf life investigation were performed to further demonstrate practical utility. The developed system demonstrates an alternative detection approach for distance-based PADs enabling fast (~ 10 min), quantitative, and straightforward assays.

Introduction

Research and development of analytical devices fabricated with paper has grown rapidly in recent years. Following the rediscovery of patterned paper as a useful analytical platform by

Correspondence to: Charles S. Henry.

†Electronic Supplementary Information (ESI) available: Design of the 3D-printed device, device components of the distance-based detection by color screening and their assembly process, operational procedure of the distance-based detection by color screening, photographs of filtering magenta color printed on a transparency film, detailed characterization procedure of the color filter, quantitative evaluation of filtering color intensity gradient printed on a transparency film, photographs of inspection window in Ni sensing, summary of recovery rate of Ni detected by user test, certified content of metals in the welding fume sample used in this work, cost calculation of the paper device. See DOI: 10.1039/x0xx00000x

Conflicts of interest

There are no conflicts to declare.

the Whitesides' group in 2007,[1] a myriad of detection approaches (*e.g.* colorimetry,[2] electrochemistry,[3] fluorescence,[4] chemiluminescence,[5] electrochemiluminescence,[6] surface enhanced Raman spectroscopy[7]) have been introduced. Because of the abundance of signal detection motifs and attractive features of patterned paper substrates (low-cost, disposability, power-free sample transportation and white background, among others), paper-based analytical devices (PADs) are currently used in a wide range applications such as medical diagnosis,[8–13] environmental assessment,[8–10, 13–15] and food safety monitoring.[8–10, 16, 17]

Patterning paper substrates allows direction-controlled (and branched, as needed) transport of a fluid sample, differentiating PADs from classical test strips such as litmus paper and lateral flow assays. This advantage of PADs provides functionalities, including the ability to perform multiplexed assays and automation of multi-step assay procedures from a single sample application. It also gave rise to a new class of optical signal detection motifs which do not rely on color intensities as is typical for many PADs and commercial paper-based tests (*e.g.* pH test strip, urine dipstick). These unique signaling methods include "counting" the number of colored paper regions on a PAD,[18–22] "timing" an event (*e.g.* coloring of a paper spot) on a PAD,[18, 23–25] and "reading" text directly reporting the assay result from the paper substrate.[26–30]

Another promising detection strategy for paper-based devices is the visual inspection of "distance" that a colored substrate has travelled in a microfluidic paper channel.[31, 32] Without the need for any signal readout instruments, quantitative analysis is achievable in a straightforward method similar to reading analog thermometers. This method has been demonstrated in a broad range of applications including the detection of metals,[33–39] biological proteins,[40, 41] nucleosides,[34, 42, 43] nucleic acids,[44, 45] haematocrit,[46] drug[34, 42, 43] and tumor markers.[47] Analyte concentration-dependent length of a colored band on paper has been conventionally achieved either by analyte depletion during capillary-based sample liquid transport within a paper microchannel,[31, 33, 35–40, 44, 45, 47] or by changing the capillary flow speed influenced by the concentration of analyte in the sample.[34, 41–43, 46] However, despite the simplified and quantitative nature of distance-based detection, the mechanism relies on capillary action within a microfluidic channel in heterogeneous filter paper substrates which leads to low precision of the assays, as indicated by mean relative standard deviations as high as 20%.[33, 37, 40] In addition, the slow process of capillary force-based sample transport necessitates extended analysis time for assay completion (45 min[33] or hours[37] for several centimeters of channel length).

This work describes a new "dip-and-read" detection motif to achieve quantitative and instrument-free chemical analysis on a paper-based device that addresses the drawbacks of conventional distance-based detection. To achieve a "dip-and-read" paper-based device that has distance-based quantification, a classical colorimetric indicator is deposited onto a filter paper substrate as a line by means of inkjet-printing.[10, 48, 49] An analyte concentration-dependent "color intensity" change of the line-shaped colorimetric indicator can be converted to "length" by isolating the "visible" section of the indicator line. For the conversion from color intensity to length, a color filter was made using a laser-printed transparent sheet. This color filter is overlaid as a "mask" to screen a part of the line-shaped colorimetric indicator. In the previous literature, color screening of an indicator by a colored

film has been applied to the semi-quantitative detection of urinary protein using text-based signalling.[30] In this work, quantitative distance-based detection has been enabled by using a color filter with a printed continuous color gradient. By using a “dip-and-read” approach, the proposed method significantly reduces the impact of capillary flow within a microfluidic paper channel, resulting in reduced chance of errors and assay time.

Herein, a new type of distance-based paper device has been developed for the quantification of nickel (Ni) to demonstrate the analytical performance of the proposed method. Occupational exposure to air polluted with harmful metals increases the risk of cardiopulmonary and respiratory diseases and even early mortality.[50] Additionally, inhalation of fumes containing Ni is regarded as a factor causing lung and nasal cancers and provoking asthma.[51, 52] Conventional analytical methods such as inductively coupled plasma-mass spectrometry[53] and atomic absorption spectrometry[54] have good selectivity and detection sensitivity. However, these methods have expensive running costs (typically > $100 per sample), require a trained operator, and necessitate sophisticated and bulky instruments, limiting their use in routine environmental monitoring. In this work, the proposed paper-based device has been applied to Ni quantitation in a welding fume sample as a low-cost and user-friendly alternative to traditional techniques. In addition to completing an interference study and evaluating storage stability, a result comparison between readout tests using the proposed approach and conventional visual color intensity comparison has been performed for analytical performance assessment. Readout results by multiple independent users showed improved analytical performance of the current approach over the color intensity comparison method and previously reported distance-based PADs.

Experimental section

Materials and instruments

Iron(II) sulfate heptahydrate, zinc(II) nitrate hexahydrate, aluminum(III) sulfate hydrate, vanadium(III) chloride, chromium(III) chloride hexahydrate, cobalt(II) chloride hexahydrate, copper(II) sulfate pentahydrate, sodium fluoride, tris(hydroxymethyl)aminomethane and ammonium acetate were purchased from Sigma-Aldrich (St. Louis, MO). Lead(II) nitrate, magnesium(II) chloride hexahydrate, cadmium(II) nitrate tetrahydrate, calcium(II) chloride dihydrate, iron(III) nitrate nonahydrate, manganese(II) chloride tetrahydrate, potassium dichromate(VI), sodium carbonate, hydrochloric acid and isopropyl alcohol were purchased from Fisher Scientific (Pittsburgh, PA). Nickel(II) sulfate hexahydrate was purchased from Acros Organics (Morris Plains, NJ). Mercury(II) chloride was purchased from Alfa Aesar (Ward Hill, MA). Dimethylglyoxime was purchased from Fluka (St. Louis, MO). Nitric acid was purchased from EMD Millipore (Billerica, MA). Ultrapure water (>18 MΩ cm) was obtained from a Milli-Q water purification system (EMD Millipore) and used for the preparation of all solutions. Whatman grade 3MM Chromatography filter paper sheet (46 × 57 cm^2) was purchased from GE Healthcare (Buckinghamshire, UK) and cut into letter size before use.

Patterning of hydrophobic wax onto filter paper was performed by a ColorQube 8870 printer (Xerox, Norwalk, CT). A thermally actuated Canon PIXMA MG2525 inkjet printer (Canon, Tokyo, Japan) was used for the deposition of the nickel colorimetric assay reagents. For this

purpose, the standard Canon black ink cartridge (Canon PG-245 FINE Cartridge) was cut open and the sponge inside was removed, followed by thorough washing with copious amounts of ultrapure water.

Fabrication of paper-based analytical device

The outline and photograph of a single paper-based analytical device (PAD) for Ni detection are shown in Figures 1a and b, respectively. A letter-sized filter paper sheet was first fed into the wax printer to pattern the hydrophobic barrier defining the hydrophilic sensing paper region designed with PowerPoint (Microsoft), followed by heating at 150 °C on an Isotemp hotplate (Fisher Scientific). To diffuse the molten wax throughout the paper thickness, each side of the filter paper was heated for 4 min. Next, 70 μL of an aqueous solution containing 0.3 M sodium fluoride and 1.2 M ammonium acetate was pipetted onto the entire sensing region as masking agents, followed by complete drying at room temperature. A solution of 20 mM dimethylglyoxime (DMG) and 10 mM tris base prepared in H_2O/isopropyl alcohol (60/40 vol%) was inkjet-printed as a 0.4 mm-wide line by the Canon printer in 5 print cycles. After sandwiching the as-processed filter paper with deposited reagents by lamination films (Scotch thermal laminating pouches, 3M, St. Paul, MN), hot lamination was performed on a TruLam TL-320B laminator at 120 °C. During the lamination step, a sheet of copy paper was inserted between the lamination film and the reagent-unprinted paper side to avoid their attachment, resulting in lamination of the paper side with the inkjet-printed colorimetric assay reagents. Finally, the letter size sheet was cut into 48 individual PADs.

Fabrication of 3D-printed device

A 3D-printed device for the distance-based detection was designed with Tinkercad software (Autodesk, San Rafael, CA) and fabricated with an Objet30 Prime 3D-printer (Stratasys, Eden Prairie, MN). A photograph after assembly and the detailed design and assembly process of the 3D-printed device are shown in Figure 1c and Figures S1 and S2 of the Electronic Supplementary Information, respectively. A color-printed transparency film for screening the color of the $Ni(DMG)_2$ complex on the PAD was fabricated by printing toner on an overhead projector transparency film (Apollo, Lincolnshire, IL) with a LaserJet Pro 400 Color M451dn laser printer (HP, Palo Alto, CA).

Window-sliding Ni assay

The operational procedure of the window-sliding detection approach is shown in Figure S3. Briefly, the PAD was first dipped in 10 mL of sample solution in a cylindrical plastic tube and removed quickly. After blotting the excess sample liquid with a Kimwipe tissue paper and drying at room temperature for approximately 10 min, the PAD was inserted into the 3D-printed device. For the quantification of the sample Ni concentration, the handle was moved upward from the lowest position of the 3D-printed device (refer to “Sliding direction” in Figure 1c) until a vertical line derived from the colored $Ni(DMG)_2$ complex becomes visible in the rectangular window (“Inspection window” in Figure 1c), with a sheet of copy paper placed under the 3D-printed device as a background.

Interference study

Interference from foreign metals including Mg(II), Al(III), Ca(II), V(III), Cr(III), Cr(VI), Mn(II), Fe(II), Fe(III), Co(II), Cu(II), Zn(II), Cd(II), Hg(II) and Pb(II) was studied. For this purpose, aqueous samples with various mass ratios between Ni and a single foreign metal were prepared to identify the maximum ratio giving no significant interference as compared to a control (interfering metal-free aqueous solution containing identical mass of Ni).

Preparation of welding fume sample

A stainless steel welding fume sample certified for Cr, Fe, Mn and Ni (SSWF-1) was obtained from the Health & Safety Laboratory (Harpur Hill, Buxton, UK). Aqua regia digestion of the SSWF-1 material was performed by the method previously reported by our group[55] with a slight modification. Briefly, 4.9 mg of the SSWF-1 material was digested into 1 mL of aqua regia heated at 70 °C for 15 min. After cooling to room temperature, 1.5 mL of an aqueous sodium carbonate solution (2 M) for neutralization and 7.5 mL of water were added.

Shelf life evaluation

To evaluate the shelf life of the developed PAD, the DMG/tris ink was printed onto the entire area of the hydrophilic paper region. Except for the inkjet-printing dimension of the DMG/tris area, the PAD was prepared in an identical manner to the case of the window-sliding detection. The PADs were wrapped in aluminum foil and stored at room temperature (25 °C) or 4 °C. After storage for various time spans (1, 2, 4, 6, 8 weeks), the PADs were exposed to aqueous Ni sample solutions (0, 0.1, 0.2, 0.4, 0.6, 0.8, 1, 2 mM). An image of the dried PAD was acquired with a Xerox DocuMate 3220 scanner (color scanning mode, 600 dpi resolution). Finally, numerical color intensity values of the hydrophilic sensing region were extracted from the scanned images by using the ImageJ software (NIH, Bethesda, MD).

Results and discussion

Principle of distance-based detection by color screening

A schematic illustration of the distance-based quantification method proposed in this work is shown in Figure 2. The PAD with inkjet-printed colorimetric indicator (dimethylglyoxime: DMG) undergoes a colorimetric response upon contact with a sample solution. In this process, the inkjet-printed DMG indicator line shows a uniform magenta color development, of which the intensity is dependent on the concentration of nickel in the sample (Figure 2a). After the color development, a transparency film with a magenta color gradient of increasing intensity is overlaid as a “mask” (Figure 2b). The color film screens those parts of the magenta-colored line derived from the $Ni(DMG)_2$ complex with weaker color intensity than that of the printed magenta toner on the overlaid transparency film (Figure 2c). This mechanism allows quantification of sample Ni concentration from the visible length of the $Ni(DMG)_2$ line. The distance-based signal is acquired by observing the color intensity of the $Ni(DMG)_2$ line through a movable “inspection window” (Figure 2d). For this purpose, a 3D-printed device (Figures 1c and S2) has been designed to integrate the PAD, the color filter, and the handle for sliding the inspection window. The Ni concentration is determined by

sliding the handle until a vertical line becomes recognizable in the inspection window and by simply reading the “concentration scale marks” printed next to the color filter. A preliminary study showed that the visible length of the colored line is more clearly judged by observing a vertical line becoming visible in the confined inspection window, rather than by directly measuring the entire length of the visible part of the colored line. This reason is attributed to the fact that the presence of the colored $Ni(DMG)_2$ line under the color filter is “biased” in the absence of the inspection window, making accurate measurement of the visible length difficult.

Optimization of color filter

To determine the color gradient to be printed on a transparency sheet was as follows: 1) obtain colorimetric response of the PADs using Ni standard samples with known concentrations; 2) print toner onto a transparency film with various intensities of color of which the hue matches that of the indicator after the colorimetric reaction (magenta in this case); 3) identify the weakest filtering color intensity for each Ni concentration by the naked eye; 4) print color gradient and concentration scale marks onto a transparency film. The image in Figure 3a shows the colorimetric response of the PAD between 0–1 mM Ni. With increasing magenta color of the developed line at higher sample Ni concentration, more intense filtering magenta color on the transparency film was required. Figure 3b summarizes the identified weakest print color value settings and the resulting print color to hide (“screen”) the developed $Ni(DMG)_2$ line at each Ni concentration. A photograph of filtering magenta color printed onto the transparency film with various intensities is shown in Figure S4 of the ESI. It should be noted that the optimal print color values in Figure 3b are specific for the laser printer used in this work and dependent on the printer model to be employed for creating the color filter. Based on the relationship between the Ni concentration and the minimum intensity of the overlaid filtering color, magenta-colored toner with an intensity gradient was printed onto the transparency sheet (Figure 3c). It should be noted that the concentration scale marks start from 0.2 mM, since the developed $Ni(DMG)_2$ line is visible only at 0.2 mM or higher concentration of Ni in the sample solution. The detailed profile of the printed gradient and its agreement with the optimal color identified in step 3) are described in the ESI and Figure S5.

Aqueous standard sample analysis

After color filter optimization, distance-based Ni quantification by the window sliding method was performed on samples with various Ni concentrations. The images in Figure 4a show the case of a 0.5 mM Ni sample analysis as an example (see Figure S6 for other Ni concentrations). The resulting magenta line becomes visible as the color intensity of the overlaid screening film was reduced by sliding the inspection window. Quantitative Ni detection was enabled by identifying the position of the sliding handle where the $Ni(DMG)_2$ line was first recognized in the inspection window. Figure 4b shows the correlation between the Ni concentration (horizontal axis) and the results from the scale marks on the 3D printed sample holder (vertical axis). Accurate quantitative analysis was achieved as demonstrated by a slope close to unity (1.004) and good linearity (R^2 value of 0.995). In addition, the relative standard deviations ranged from 2.1–13% with 8.0% average. However, considering the current detection approach is based on visual observation of a colored line in an

inspection window, the assay result might inherently be biased. In this context, the proposed quantification approach was validated by having multiple independent users quantify Ni concentration using the proposed method.

Ni quantification in welding fume sample by multiple users

To further investigate the analytical performance of the developed PAD, the Ni content in a welding fume sample was independently quantified by multiple users. The certified metal content for the SSWF-1 reference material is shown in Table S1. The resulting digested solution (0.31 mM of Ni) as well as three additional samples spiked with Ni to 0.61, 0.81 and 0.91 mM were subject to Ni determination by 8 volunteer users. Before testing, the users were instructed on the readout method using the line visibility based on the case of a 0.6 mM standard sample as a reference. For analytical performance comparison, Ni concentrations were measured by visual comparison of the sample color intensity with that of a read guide prepared by PADs exposed to aqueous Ni standards of known concentration (devices identical to those in Figure 3a). Figures 5a and 5b show the readout results of Ni concentrations by 8 independent users obtained from the developed distance-based approach and visual color intensity comparison, respectively. For easier result interpretation, the recovery rate calculated from the data in Figure 5 is summarized in Table 1 and Figure S7 (bar graph format). A notable difference between the proposed method and the colorimetric approach was observed in the accuracy of the unspiked sample, where the readout value based on the visual color intensity comparison was generally lower than the true value (0.31 mM of Ni). This reason might be attributed to minor color blurring that was observed in the developed $Ni(DMG)_2$ line, making the overall color intensity weaker than that of the color read guide with the closest concentration (*i.e.* 0.3 mM). On the other hand, we postulate that the distance-based detection approach was less influenced by this phenomenon because the highest color intensity of the $Ni(DMG)_2$ line was maintained at its center and was not impacted by color blurring.

Table 2 summarizes the analytical performance comparison between the distance-based detection motif by color screening and the naked eye-based color intensity comparison method. It should be noted that accuracy and precision are defined as the means of absolute percentage error of Ni quantification and relative standard deviations, and thus, smaller percentage values represent better performance. Table 2 shows that the proposed distance-based detection method improves the overall readout accuracy and precision as compared to the color intensity comparison-based approach. In addition, a significant improvement of precision has been achieved from a distance-based PAD for Ni quantification relying on capillary action-based analyte depletion within a paper microchannel (23.5% precision).[33] One possible explanation for this improvement is that the developed distance-based detection motif does not involve capillary force-driven sample wicking. “Conventional” distance-based detection not using color screening relies on capillary flow, of which the reproducibility is susceptible to the heterogeneous nature of filter paper, such as the orientation direction of cellulosic fibres.[56, 57] Because the new method does not rely on capillary forces, a shortened assay time (~ 10 min) is achieved when compared to the “conventional” distance-based detection (45 min) having the same length of a detection channel (5 cm).[33] Finally, the cost of the developed PADs was calculated to be $0.011 per

device (detailed calculation is shown in Table S2), which is significantly lower than the conventional analytical techniques (>$100 per sample).

Interference study

Mn(II), Fe(III), Co(II) and Cu(II) are metals known to interfere with the DMG-based Ni assay.[58] Sodium fluoride and ammonium acetate were pre-deposited onto the entire hydrophilic area of the PAD to mask these interferences. The effect of the deposited masking reagents was evaluated with a tolerance study. The tolerance ratio identifies the maximum mass ratio between Ni and an interfering metal giving rise to change in signal of less than 10%. For these studies the Ni mass was fixed at 294 μg (0.5 mM in 10 mL sample solution). Figure 6 shows the readout of Ni concentration under various interfering conditions, and Table 3 summarizes the tolerance mass ratio of each interfering metal, respectively. The presence of Mg(II), Al(III), Ca(II), V(III), Cr(III), Cr(VI), Mn(II), Fe(II), Fe(III), Zn(II), Cd(II), Hg(II) and Pb(II) at a mass ratio of >10:1 did not affect the assay results. Thus, these metal ions do not interfere with the Ni assay at the concentrations normally found in stainless steel welding fumes. The potential interference from Mn(II) and Fe(III) has been eliminated thanks to the presence of the masking reagents pre-deposited onto the PAD. On the other hand, even with the use of the masking agents, interference from Co(II) and Cu(II) was observed at a mass ratio of 0.5. The presence of these metals at a mass ratio higher than 1 to Ni resulted in weaker color development, contradicting the fact that DMG forms a colored complex with Co(II) and Cu(II).[59] This discrepancy is explained by the fact that $Co(DMG)_2$ and $Cu(DMG)_2$, formed in competition with the complexation of DMG with Ni(II), are water-soluble[60, 61] and thus, spread within the hydrophilic paper area, resulting in weak color development of $Ni(DMG)_2$. However, the percent composition of Co and Cu rarely reaches equivalent levels to that of Ni in stainless steels,[33] and should not be an issue in the context of the application presented.

Shelf life evaluation of PAD

The long-term stability of the developed PAD was evaluated by monitoring the colorimetric response of the inkjet-printed DMG reagent to Ni concentrations after storage up to 8 weeks in the dark. Figures 7a and 7b represents the time course of the color intensity values in the RGB (red, green, blue) color coordinates after storage at room temperature (25 °C) and 4 °C, respectively. Over the tested storage period up to 8 weeks, the PAD showed no statistically signification variation in the developed red, green and blue color intensities regardless of the storage temperature. With the stable colorimetric response, the analytical performance of the elaborated distance-based detection method is expected to be fully maintained at least for 8 weeks by simple light-shielded storage condition.

Conclusions

This work demonstrates the first reported distance-based quantification mode on PADs by using the indicator color screening strategy. The “dip-and-read” assay format eliminates the capillary flow-based analyte depletion step in a microfluidic paper channel utilized in the conventional distance-based detection motif. The results of multiple user tests of Ni quantification demonstrated improved analytical precision and shortened assay time as

compared to the previously reported distance-based PAD for Ni detection. It was also experimentally confirmed that the proposed detection approach exhibits better analytical accuracy and precision than a visual color intensity comparison method. Although the readout result of the “dip-and-read” assay is still dependent on an individual’s color recognition capacity and may be inherently biased by different users, the improved analytical accuracy and precision over the traditional visual color intensity comparison approach suggest that user-dependent variation of instrument-free colorimetric assay results has been mitigated by the proposed method. Therefore, this new distance-based quantification approach is a promising alternative signaling motif on paper-based analytical devices allowing low-cost and simple, yet quantitative precise assays. Although the current work demonstrates Ni detection by the dimethylglyoxime colorimetric indicator for proof-of-concept, the elaborated detection system is expected to be expandable to other analytical targets by changing the colorimetric indicator and the color filter.

Supplementary Material

Refer to Web version on PubMed Central for supplementary material.

Acknowledgments

K.Y. gratefully acknowledges the funding from a Research Fellowship of the Japan Society for the Promotion of Science (JSPS) for Young Scientists. C.S.H. acknowledges support from the National Institute of Occupational Safety and Health (OH010662). The authors thank the volunteers cooperating on the device user test. The authors also acknowledge Katherine Boehle and Cody Carrell of the Department of Chemistry, Colorado State University, for valuable discussions and for their help with manuscript editing.

References

1. Martinez AW, Phillips ST, Butte MJ, Whitesides GM. Angew. Chem. Int. Ed. 2007; 46:1318–1320.
2. Martinez AW, Phillips ST, Carrilho E, Thomas SW, Sindi H, Whitesides GM. Anal. Chem. 2008; 80:3699–3707. [PubMed: 18407617]
3. Dungchai W, Chailapakul O, Henry CS. Anal. Chem. 2009; 81:5821–5826. [PubMed: 19485415]
4. Carrilho E, Phillips ST, Vella SJ, Martinez AW, Whitesides GM. Anal. Chem. 2009; 81:5990–5998. [PubMed: 19572563]
5. Yu J, Ge L, Huang J, Wang S, Ge S. Lab Chip. 2011; 11:1286–1291. [PubMed: 21243159]
6. Delaney JL, Hogan CF, Tian J, Shen W. Anal. Chem. 2011; 83:1300–1306. [PubMed: 21247195]
7. Yu WW, White IM. Anal. Chem. 2010; 82:9626–9630. [PubMed: 21058689]
8. Yetisen AK, Akram MS, Lowe CR. Lab Chip. 2013; 13:2210–2251. [PubMed: 23652632]
9. Cate DM, Adkins JA, Mettakoonpitak J, Henry CS. Anal. Chem. 2015; 87:19–41. [PubMed: 25375292]
10. Yamada K, Henares TG, Suzuki K, Citterio D. Angew. Chem. Int. Ed. 2015; 54:5294–5310.
11. Fernandes SC, Walz JA, Wilson DJ, Brooks JC, Mace CR. Anal. Chem. 2017; 89:5654–5664. [PubMed: 28406607]
12. Yamada K, Shibata H, Suzuki K, Citterio D. Lab Chip. 2017; 17:1206–1249. [PubMed: 28251200]
13. Yang Y, Noviana E, Nguyen MP, Geiss BJ, Dandy DS, Henry CS. Anal. Chem. 2017; 89:71–91. [PubMed: 27936612]
14. Meredith NA, Quinn C, Cate DM, Reilly TH, Volckens J, Henry CS. Analyst. 2016; 141:1874–1887. [PubMed: 26901771]
15. Lin Y, Gritsenko D, Feng S, Teh YC, Lu X, Xu J. Biosens. Bioelectron. 2016; 83:256–266. [PubMed: 27131999]

16. Busa L, Mohammadi S, Maeki M, Ishida A, Tani H, Tokeshi M. Micromachines. 2016; 7:86.
17. Hua M, Li S, Wang S, Lu X. Micromachines. 2018; 9:32.
18. Lewis GG, DiTucci MJ, Phillips ST. Angew. Chem. Int. Ed. 2012; 51:12707–12710.
19. Karita S, Kaneta T. Anal. Chem. 2014; 86:12108–12114. [PubMed: 25423320]
20. Zhang Y, Zhou C, Nie J, Le S, Qin Q, Liu F, Li Y, Li J. Anal. Chem. 2014; 86:2005–2012. [PubMed: 24444190]
21. Karita S, Kaneta T. Anal. Chim. Acta. 2016; 924:60–67. [PubMed: 27181645]
22. Zhang Y, Gao D, Fan J, Nie J, Le S, Zhu W, Yang J, Li J. Biosens. Bioelectron. 2016; 78:538–546. [PubMed: 26684676]
23. Lewis GG, Robbins JS, Phillips ST. Anal. Chem. 2013; 85:10432–10439. [PubMed: 24074247]
24. Lewis GG, Robbins JS, Phillips ST. Chem. Commun. 2014; 50:5352–5354.
25. Zhang Y, Fan J, Nie J, Le S, Zhu W, Gao D, Yang J, Zhang S, Li J. Biosens. Bioelectron. 2015; 73:13–18. [PubMed: 26042873]
26. Li M, Tian J, Al-Tamimi M, Shen W. Angew. Chem. Int. Ed. 2012; 51:5497–5501.
27. Carrasquilla C, Little JRL, Li Y, Brennan JD. Chem. - Eur. J. 2015; 21:7369–7373. [PubMed: 25820300]
28. Li M, Cao R, Nilghaz A, Guan L, Zhang X, Shen W. Anal. Chem. 2015; 87:2555–2559. [PubMed: 25645265]
29. Li J, Macdonald J. Lab Chip. 2016; 16:242–245. [PubMed: 26621222]
30. Yamada K, Suzuki K, Citterio D. ACS Sens. 2017; 2:1247–1254. [PubMed: 28809488]
31. Cate DM, Dungchai W, Cunningham JC, Volckens J, Henry CS. Lab Chip. 2013; 13:2397–2404. [PubMed: 23657627]
32. Tian T, Li J, Song Y, Zhou L, Zhu Z, Yang CJ. Lab Chip. 2016; 16:1139–1151. [PubMed: 26928571]
33. Cate DM, Noblitt SD, Volckens J, Henry CS. Lab Chip. 2015; 15:2808–2818. [PubMed: 26009988]
34. Wei X, Tian T, Jia S, Zhu Z, Ma Y, Sun J, Lin Z, Yang CJ. Anal. Chem. 2015; 87:4275–4282. [PubMed: 25806667]
35. Rahbar M, Nesterenko PN, Paull B, Macka M. Anal. Chem. 2017; 89:11918–11923. [PubMed: 29090570]
36. Pratiwi R, Nguyen MP, Ibrahim S, Yoshioka N, Henry CS, Tjahjono DH. Talanta. 2017; 174:493–499. [PubMed: 28738613]
37. Shimada Y, Kaneta T. Anal. Sci. 2018; 34:65–70. [PubMed: 29321460]
38. Bandara GC, Heist CA, Remcho VT. Anal. Chem. 2018; 90:2594–2600. [PubMed: 29333859]
39. Gerold CT, Bakker E, Henry CS. Anal. Chem. 2018; doi: 10.1021/acs.analchem.8b00559
40. Yamada K, Henares TG, Suzuki K, Citterio D. ACS Appl. Mater. Interfaces. 2015; 7:24864–24875. [PubMed: 26488371]
41. Zhang L, Nie J, Wang H, Yang J, Wang B, Zhang Y, Li J. Anal. Methods. 2017; 9:3375–3379.
42. Wei X, Tian T, Jia S, Zhu Z, Ma Y, Sun J, Lin Z, Yang CJ. Anal. Chem. 2016; 88:2345–2352. [PubMed: 26765320]
43. Tian T, An Y, Wu Y, Song Y, Zhu Z, Yang C. ACS Appl. Mater. Interfaces. 2017; 9:30480–30487. [PubMed: 28816436]
44. Hongwarittorrn I, Chaichanawongsaroj N, Laiwattanapaisal W. Talanta. 2017; 175:135–142. [PubMed: 28841970]
45. Wang AG, Dong T, Mansour H, Matamoros G, Sanchez AL, Li F. ACS Sens. 2018; 3:205–210. [PubMed: 29336569]
46. Berry SB, Fernandes SC, Rajaratnam A, DeChiara NS, Mace CR. Lab Chip. 2016; 16:3689–3694. [PubMed: 27604182]
47. Chen Y, Chu W, Liu W, Guo X. Sens. Actuat. B: Chem. 2018; 260:452–459.
48. Komuro N, Takaki S, Suzuki K, Citterio D. Anal. Bioanal. Chem. 2013; 405:5785–5805. [PubMed: 23677254]

49. Li J, Rossignol F, Macdonald J. Lab Chip. 2015; 15:2538–2558. [PubMed: 25953427]
50. Pope CA III, Thun MJ, Namboodiri MM, Dockery DW, Evans JS, Speizer FE, Heath CW Jr. Am. J. Respir. Crit. Care Med. 1995; 151:669–674. [PubMed: 7881654]
51. United States Environmental Protection Agency. [accessed February 8, 2018] Health Effects Notebook for Hazardous Air Pollutants, Nickel Compounds. https://www.epa.gov/sites/production/files/2016-09/documents/nickle-compounds.pdf
52. Stacey P, Butler O. Ann. Occup. Hyg. 2008; 52:287–295. [PubMed: 18453528]
53. Goullé J-P, Mahieu L, Castermant J, Neveu N, Bonneau L, Lainé G, Bouige D, Lacroix C. Forensic Sci. Int. 2005; 153:39–44. [PubMed: 15979835]
54. Taylor A, Branch S, Halls DJ, Owen LMW, White M. J. Anal. At. Spectrom. 2000; 15:451–487.
55. Mettakoonpitak J, Miller-Lionberg D, Reilly T, Volckens J, Henry CS. J. Electroanal. Chem. 2017; 805:75–82.
56. Tenda K, Ota R, Yamada K, Henares TG, Suzuki K, Citterio D. Micromachines. 2016; 7:80.
57. Ota R, Yamada K, Suzuki K, Citterio D. Analyst. 2018; 143:643–653. [PubMed: 29185559]
58. Gazda DB, Fritz JS, Porter MD. Anal. Chim. Acta. 2004; 508:53–59.
59. Onsunlaja AA, Ndahi NP, Ameh JA. Afr. J. Biotechnol. 2009; 8:4–11.
60. Sharpe AG, Wakefield DB. J. Chem. Soc. 1957:281–285.
61. Caton JE, Banks CV. Talanta. 1966; 13:967–977. [PubMed: 18959961]

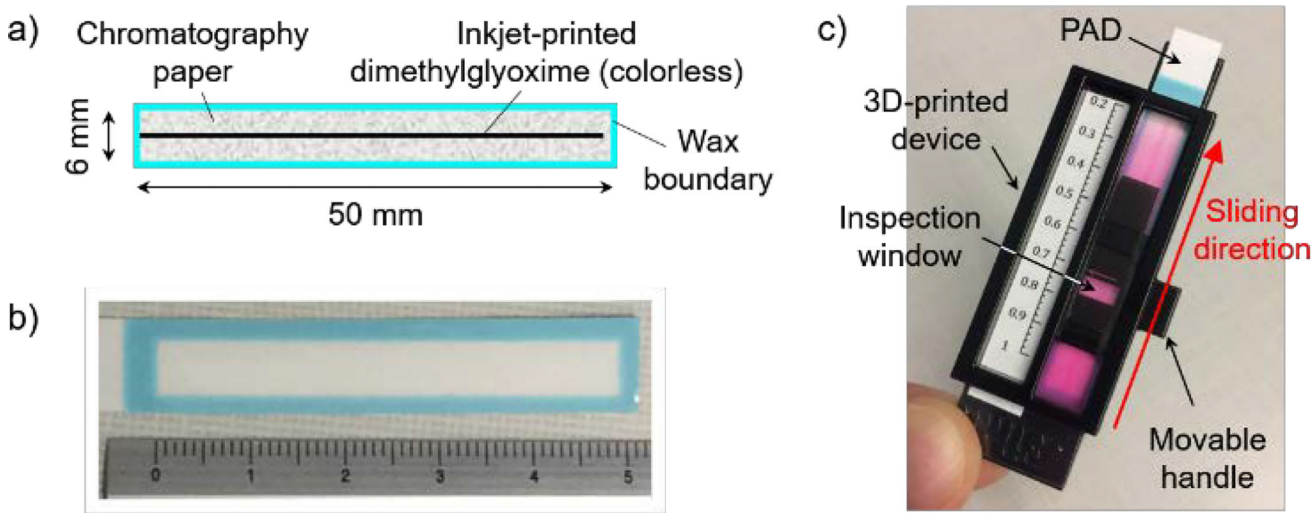

Figure 1.

a) Schematic outline and dimension of a single paper-based analytical device (PAD) for Ni detection; b) photograph of the PAD; c) photograph of the assembled 3D-printed device.

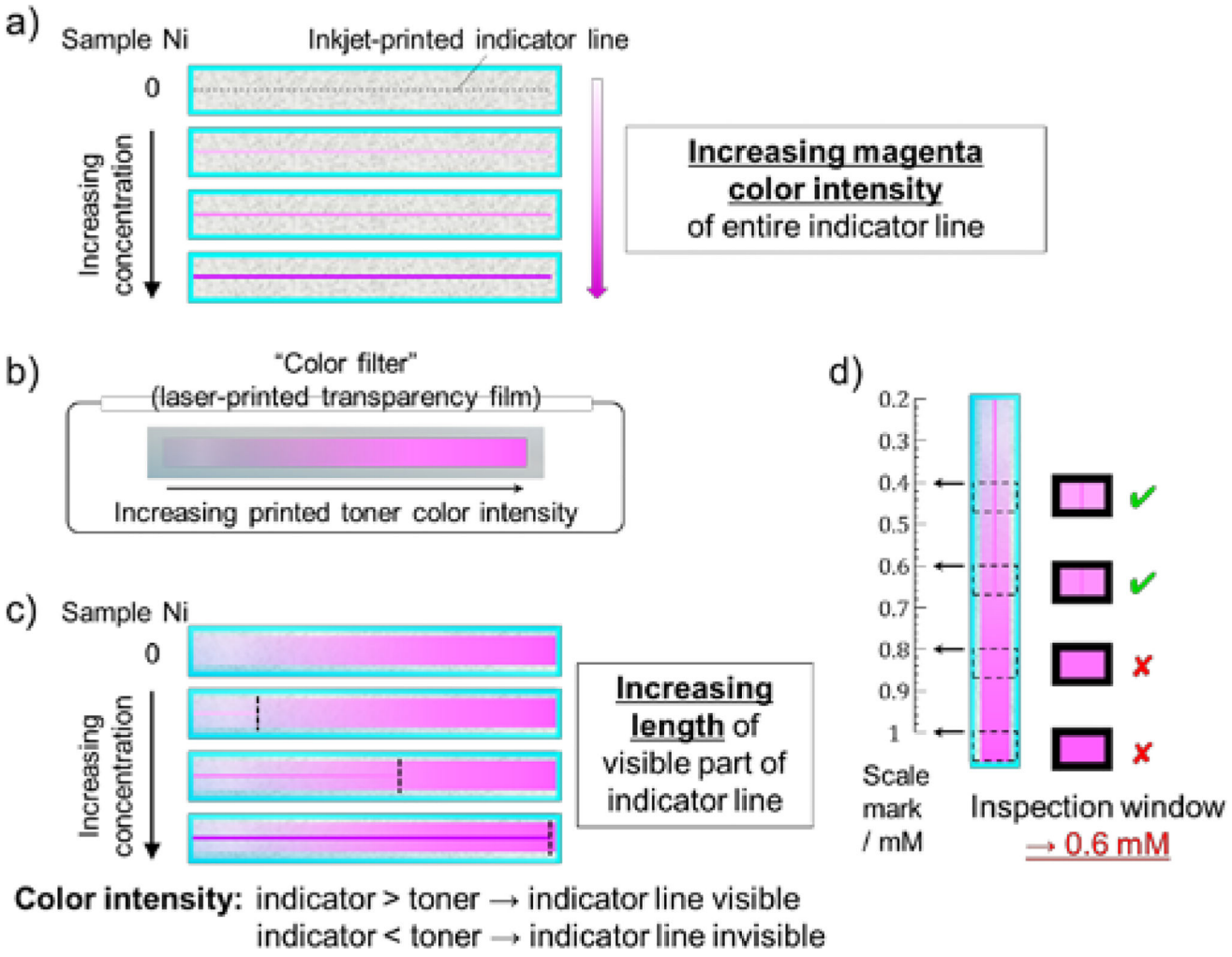

Figure 2.

A schematic illustration describing the working principle of the distance-based quantification method by color screening: a) colorimetric indicator inkjet-deposited onto the PAD in the shape of a line shows sample analyte (Ni) concentration-dependent color intensity increase; b) an overlaid transparent color filter with an intensity gradient of laser-printed toner; c) screening of a part of the developed line on the PAD by the overlaid transparent color filter to display sample analyte concentration-dependent length of the visible band; d) sample analyte concentration is quantified by comparing the lowest position of the inspection window allowing visual recognition of a band and the adjacent scale marks.

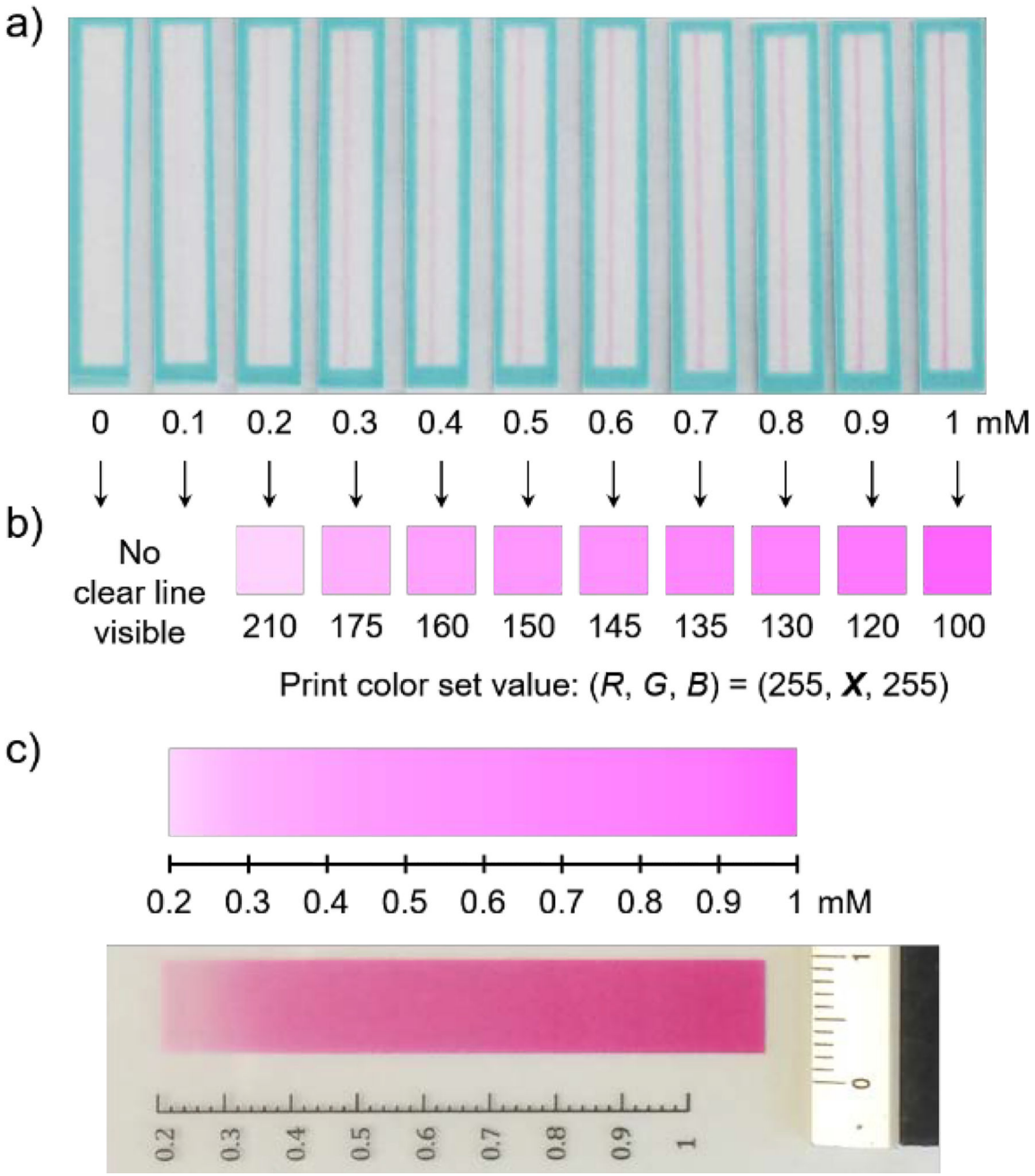

Figure 3.

a) Ni concentration-dependent color change of the PAD; b) pre-set colors on a computer and print color value settings of the filtering color for each Ni concentration; c) pre-set color gradient and actual photograph of the color filter.

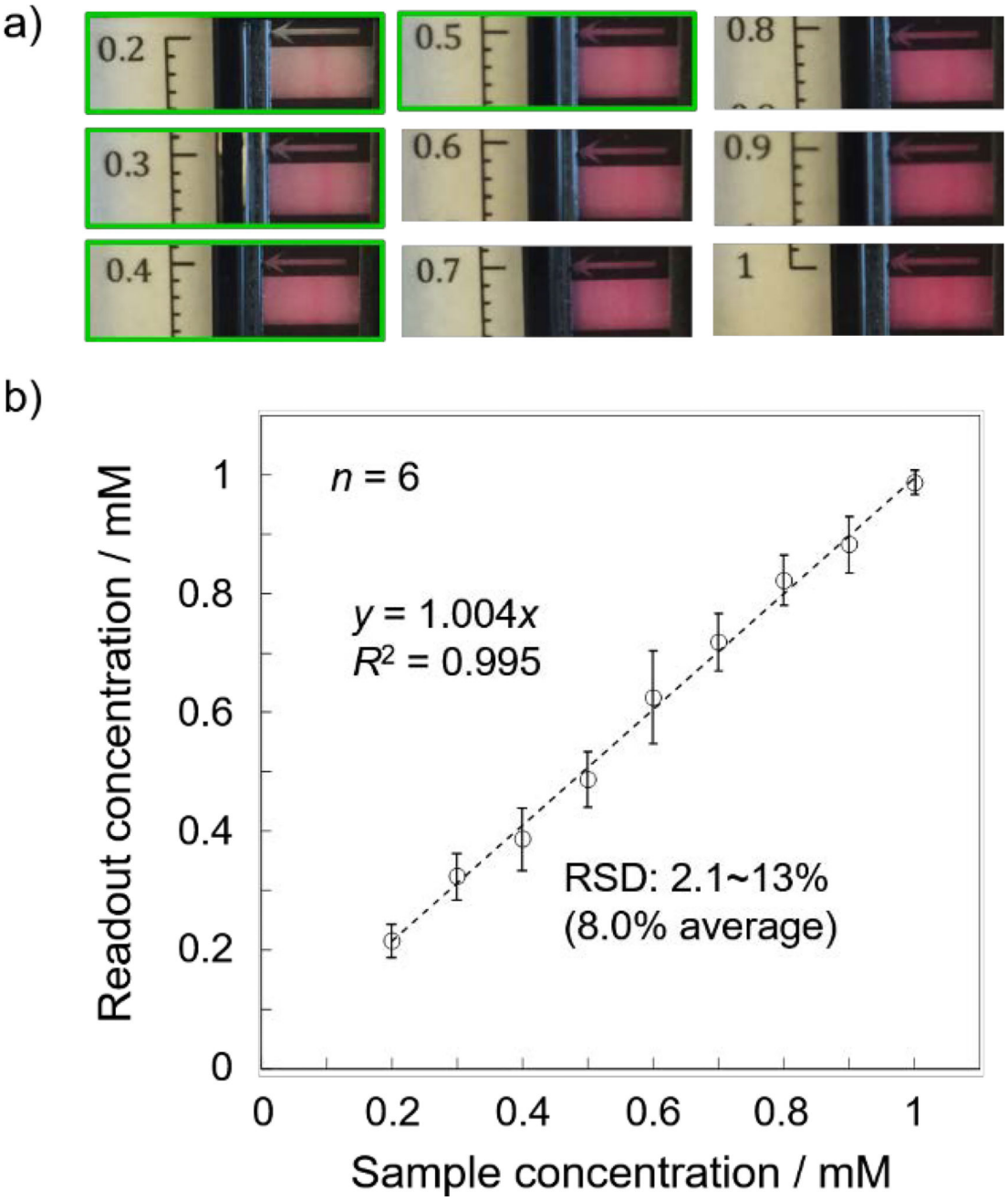

Figure 4.

Demonstration of distance-based Ni sensing by the window sliding method: a) actual photographs of the inspection window at various scale mark positions. The result shows the case of a 0.5 mM Ni sample concentration as an example (results of other Ni concentrations are shown in Figure S5 of the ESI). The image boxes highlighted by the green outline show the visible state of the vertical line inside the inspection window. Note that the light blue lines seen to the left of the windows are shadows of a part of the 3D-printed device; b) correlation between the sample Ni concentration and the readout values from the scale marks of the device.

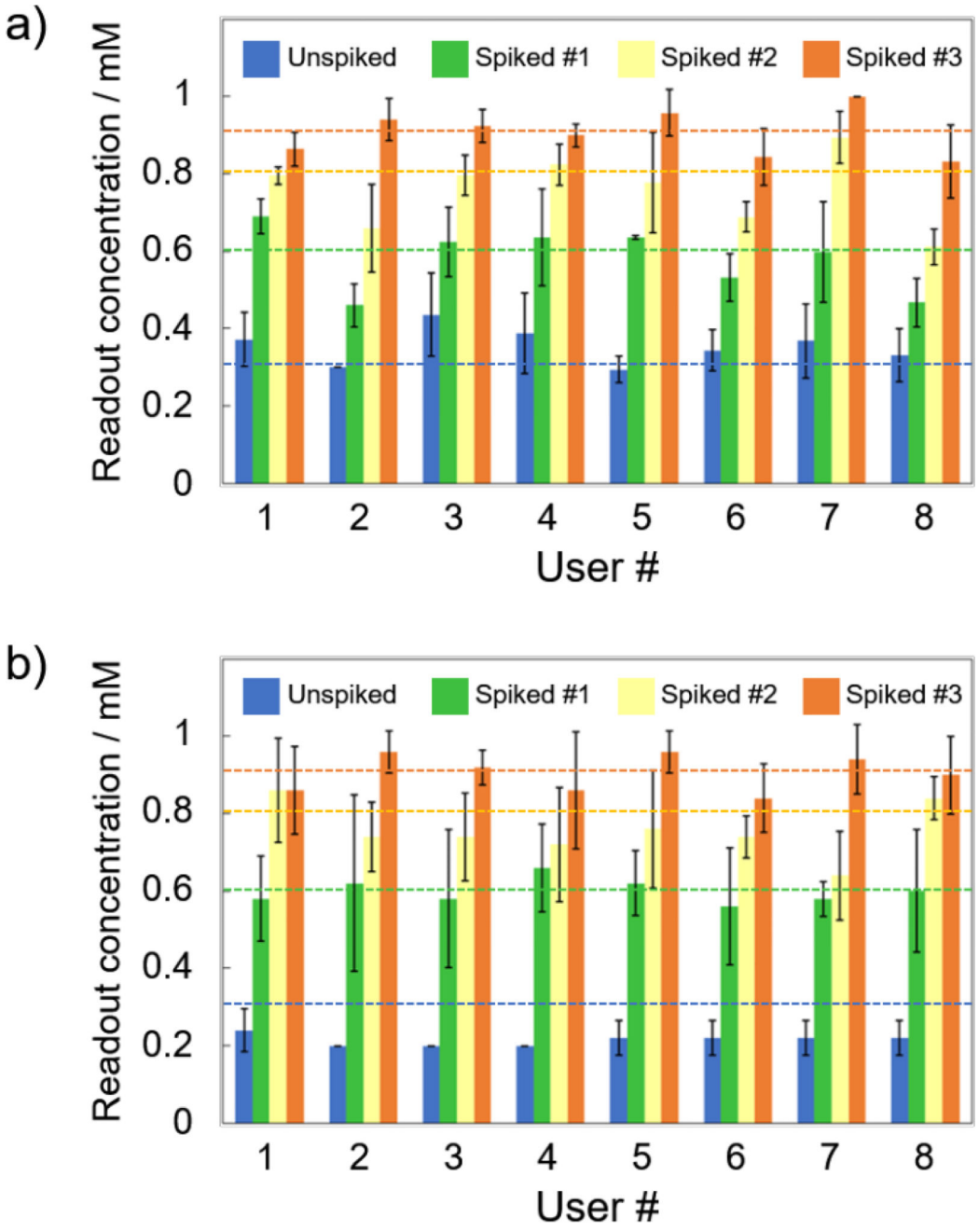

Figure 5.

Readout results of Ni concentration digested from welding fume by using a) the distance-based method and b) the color intensity comparison method. The data represent the average and standard deviations of 5 independent measurements by 8 volunteer users. The “Unspiked”, “Spiked #1”, “Spiked #2” and “Spiked #3” samples contain 0.31, 0.61, 0.81 and 0.91 mM of Ni, as indicated by the dotted horizontal lines with a color corresponding to the legend.

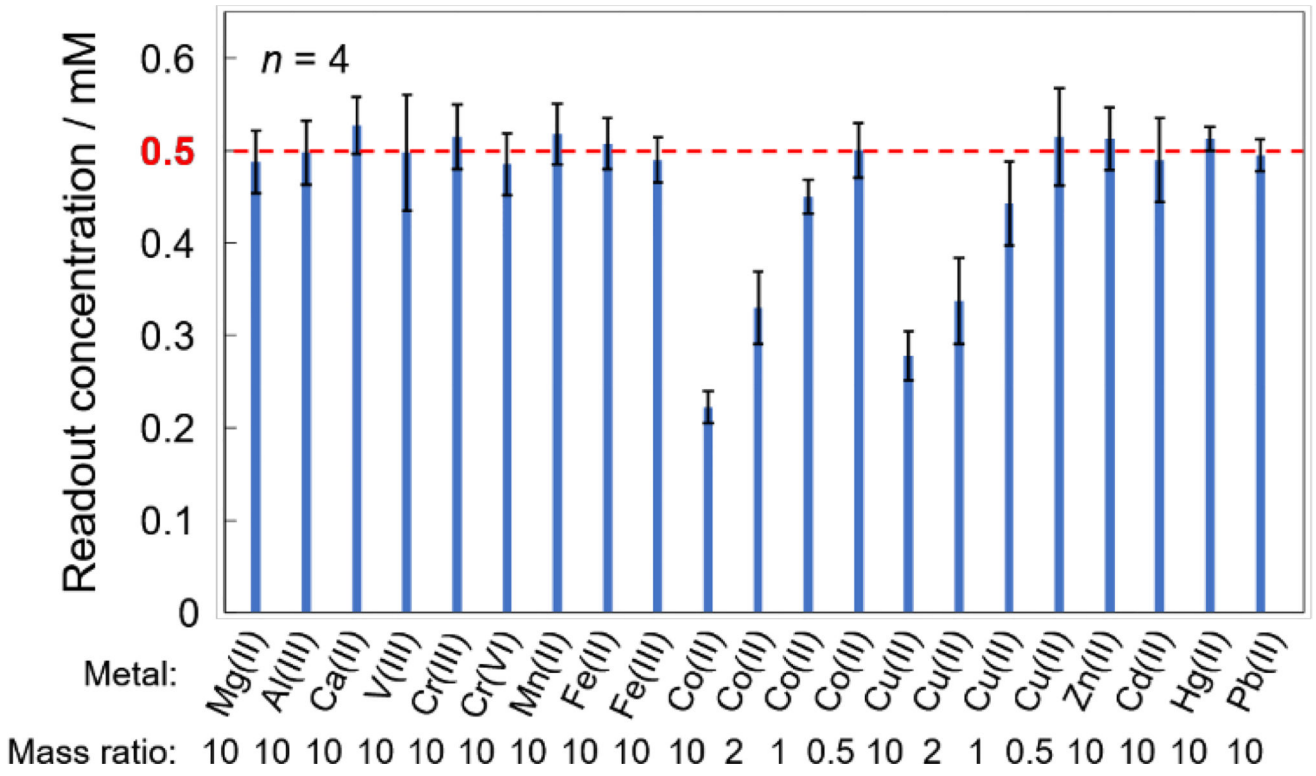

Figure 6.

Result of Ni concentration readout in the presence of Ni and interfering metals. The amount of Ni was fixed at 0.5 mM (294 μg in 10 mL of sample), whereas the amount of the interfering metals was varied as indicated at the bottom of the graph. The dotted red line highlights the true readout value (0.5 mM).

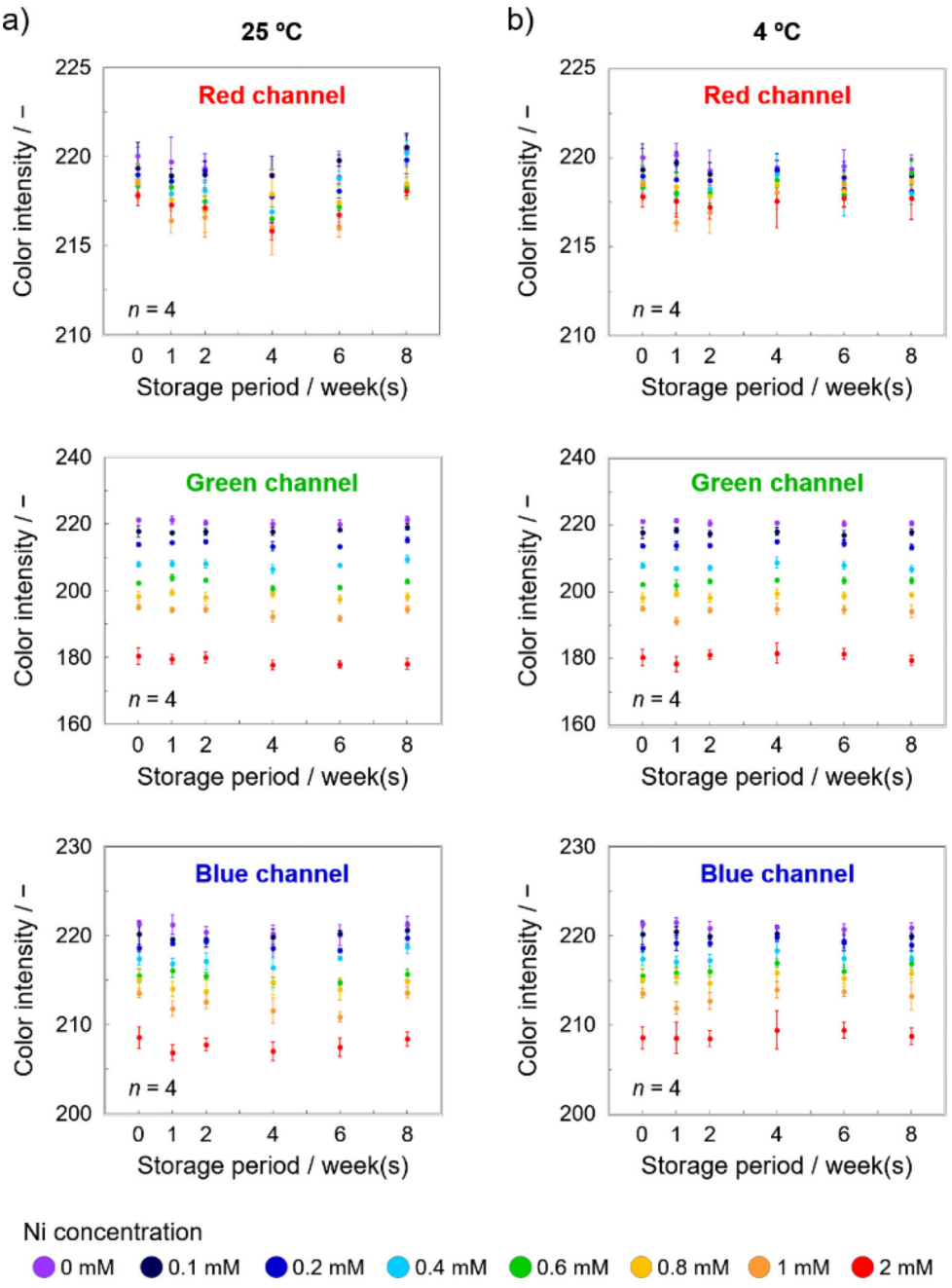

Figure 7.

Shelf life evaluation of the DMG-based colorimetric detection system for Ni. After storage for various time periods, the PADs with inkjet-printed DMG were exposed to Ni solution of various concentrations and digital color analysis was performed. The PAD was stored at a) room temperature (25 °C) and 4 °C. The graphs represent analyzed color intensity values of red (top row), green (middle row) and blue (bottom row), respectively.

Table 1

Results of recovery rate (%) of the user test-based quantification of Ni digested from a welding fume. The data reflect mean ± standard deviation obtained from 5 independent measurements by a) the proposed distance-based method and b) naked eye-based color intensity comparison.

a)

Sample	User #1	User #2	User #3	User #4	User #5	User #6	User #7	User #8
Unspiked	120 ± 23	97 ± 0	141 ± 35	125 ± 34	95 ± 11	111 ± 17	119 ± 31	107 ± 22
Spiked #1	113 ± 7.3	75 ± 9.0	102 ± 15	104 ± 21	104 ± 0.9	87 ± 10	98 ± 21	77 ± 10
Spiked #2	98 ± 2.7	81 ± 14	98 ± 6.4	102 ± 6.6	96 ± 16	85 ± 4.8	110 ± 8.3	76 ± 5.7
Spiked #3	95 ± 4.8	103 ± 6.0	102 ± 4.8	99 ± 3.2	105 ± 6.6	93 ± 8.1	110 ± 0	91 ± 10

b)

Sample	User #1	User #2	User #3	User #4	User #5	User #6	User #7	User #8
Unspiked	77 ± 18	65 ± 0	65 ± 0	65 ± 0	71 ± 14	71 ± 14	71 ± 14	71 ± 14
Spiked #1	95 ± 18	102 ± 37	95 ± 29	108 ± 19	102 ± 14	92 ± 25	95 ± 7.3	98 ± 26
Spiked #2	106 ± 17	91 ± 11	91 ± 14	89 ± 18	94 ± 19	91 ± 6.8	79 ± 14	104 ± 6.8
Spiked #3	95 ± 13	105 ± 6.0	101 ± 4.9	95 ± 17	105 ± 6.0	92 ± 9.8	103 ± 9.8	99 ± 11

Table 2

Analytical performance comparison between the proposed distance-based detection and the visual color intensity comparison method.

Parameter	Distance	Visual color intensity
Mean recovery[a]	101%	90%
Accuracy[b]	10.5%	12.2%
Precision[c]	11.2%	14.9%

[a] Expressed as the average value of the recovery rates shown in Table 1;

[b] expressed as the mean absolute percentage error of the recovery rates shown in Table 1;

[c] expressed as the mean of the relative standard deviations of measured Ni concentration values.

Table 3

Interferences from foreign metals.

Interfering ion	Tolerance mass ratio[a]
Mg(II)	≥10
Al(III)	≥10
Ca(II)	≥10
V(III)	≥10
Cr(III)	≥10
Cr(VI)	≥10
Mn(II)	≥10
Fe(II)	≥10
Fe(III)	≥10
Co(II)	0.5
Cu(II)	0.5
Zn(II)	≥10
Cd(II)	≥10
Hg(II)	≥10
Pb(II)	≥10

[a]Tolerance mass ratio was defined as the maximum mass ratio between Ni and an interfering metal giving rise to change in signal of less than 10% based on the result in Figure 6.